Bulg. J. Phys. **39** (2012) 150–164

Modelling of Nonlinear Interaction of Rb^{87} Atoms with Polarized Radiation

V. Polischuk[1], **V. Domelunksen**[1], **E. Alipieva**[2], **G. Todorov**[2]

[1]V.A. Fock Physics Institute, St. Petersburg State University,
198903 St. Petersburg, Russia
[2]Institute of Electronics "Acad. E. Djakov", Bulgarian Academy of Sciences,
72 Tzarigradsko Chaussee, 1784 Sofia, Bulgaria

Received *12 March 2012*

Abstract. The ultra narrow resonances, obtained by means of polarization spectroscopy of alkali atoms, originate from the destruction of the laser-induced coherence in the ground state. In the case of single-frequency, near resonance excitation and suitable geometry the well-known ground state Hanle effect is observed. Coherent population trapping in Hanle configuration is a nonlinear modification of this effect, observed in the fluorescence from the upper level. The ground state coherence is transmitted from the laser field and higher rank polarization moments are created. Using the irreducible tensor operator formalism programs for numerical modelling of this effect has been developed and presented here. The velocity distribution of the atoms, the Gaussian distribution of the laser beam, stray magnetic field, and the experimental geometry are taken into account. The scheme of conversion of the octupole ($\kappa = 3$) and hexadecapole ($\kappa = 4$) polarization moments (PM) through the laser and magnetic fields into the upper level quadropoles f_q^2 is proposed. The conversion of the high-rank polarization moments (PM) into observable components is also discussed. The results of the modelling are compared with the measured ones at different experimental conditions.

PACS codes: 32.80Xx, 32.70.Jz, 32.50.+d

1 Introduction

The ultra-narrow resonances, obtained in polarization spectroscopy of alkali atoms, originate from the destruction of the laser-induced coherence in the ground state. In the case of a single frequency, near-resonant excitation and a suitable geometry of irradiation and observation by scanning a weak magnetic field the well-known ground state Hanle effect is observed [1,2]. This effect can be considered as a particular case of Coherent Population Trapping (CPT) [3] on the degenerate ground states Zeeman sublevels. The laser field transfers

the coherence created in the ground state to the upper level resulting in narrow magnetic resonances observed in the fluorescence. The parameters of these resonances – shape, amplitude and sign and their dependence on the excitation and registration conditions have been investigated theoretically and experimentally in numerous works. In most of them the theoretical modelling is based on solving the optical Bloch equations, as a rule in adiabatic approximation. Different works take into account also: the velocity distribution of the atoms [4,5], the non-uniform distribution of the laser beam intensity [6,7], high-rank polarization moments [8-11]. The influence of the laser power density and polarization of the exciting field on the amplitude, shape and sign of the CPT resonances have been investigated in different schemes of excitation and detecting.

Recently a lot of papers have been dedicated to the so called bright resonance or EIA (electromagnetically induced absorption). Conversion of dark to a bright resonance was observed in dependence on the experimental conditions in the same system of levels. In a very recent work [12] M. Auzinsh and coworkers performed a systematic experimental and theoretical investigation of the dark and bright CPT resonances in a Hanle configuration. Quantitative agreement of theory and experiment was obtained for a partially overlapped hyperfine Rb levels. A more detailed description of a method for numerical solution of the optical Bloch equations, accepted approximations and their validity as well as possible errors for Rb atoms, are given in [13]. The calculations presented are carried out for strong magnetic fields ($\pm$15 Ga), while the ultra-narrow resonances are concentrated in the region smaller than 1 mGa.

Our brief review of selected works shows the variety of investigations of the parameters of the nonlinear interference resonances only in one direction – CPT on degenerated Zeeman sublevels of the ground state. Knowledge of the role of different processes and experimental conditions in the creation and registration of the optical signal is important for applications of the CPT resonances – in magnetometry for instance. The numerical experiments allow modelling the influence of different parameters on the resonance. On the other hand comparison with experiment helps to improve the model developed.

In this report a model for Matlab based description of the CPT-resonances in Hanle configuration is presented. The numerical calculations take into account the high rank polarization moments (HRPM) influence, the velocity distribution of the atoms, the Gaussian distribution of the laser beam intensity, stray magnetic fields, and the experimental geometry. The irreducible tensor operator (ITO) formalism was used. The approach accepted by us is based on the algebraization of the system of equations in this formalism, for a given hyperfine transition and geometry of excitation. Sparse matrix building enables to avoid errors when a large number of equations are written. The results of the computations are compared with the measured ones at corresponding experimental conditions.

2 Equations

The theoretical analysis of the CPT resonances obtained in Hanle effect configuration and observed in fluorescence is based on the standard semiclassical description of the atomic system by the statistical operator $\hat{\rho}$ in density matrix representation. The Hamiltonian of the system $\hat{H}$ is a sum of the operator of the free atom $\hat{H}_0$, the operator of magnetic-dipole interaction $\hat{H}'$ and the operator of interaction with the laser radiation $\hat{V}$. Terms describing the atomic relaxation and excitation transfer are added to the Liuville equation

$$\dot{\hat{\rho}} = -\frac{i}{h}\left[\hat{H}, \hat{\rho}\right] + \left(\dot{\hat{\rho}}\right)_{\text{relax}} + \left(\dot{\hat{\rho}}\right)_{\text{tr}} + \hat{N}\,, \tag{1}$$

where $\hat{H} = \hat{H}_0 + \hat{H}' + \hat{V}$.

In weak magnetic field the magnetic-dipole interaction is smaller than the hyperfine splitting and the hyperfine splitting can be included in the main Hamiltonian $\hat{H}_0$. In this case the magnetic-dipole operator can be written as: $\hat{H}' = \mu_0 g_{F_s}\left[\vec{F}_s, \vec{H}\right]$, where μ_0 is the Bohr magneton, g_F – the Lande factor, F_s is the total momentum of the atom in the s state, ($s = f$, φ), and $\vec{H}$ – the vector of the magnetic field. The complete magnetic field includes the scanned magnetic field and a stray laboratory magnetic field H_{str}.

The operator of interaction with the laser radiation $\hat{V}$ is described with the scalar product of the vector operator of the dipole moment $\hat{d}$ and the electric vector of the light $\vec{E}$:

$$\hat{V} = -\left(\vec{d}, \vec{E}\right), \qquad \vec{E} = E\vec{e}_Q \exp\{-i(\omega_{\text{las}}t - kz)\} + c.c.\,, \tag{2}$$

where: $e_Q(Q = 0, \pm 1)$ are the linear and the circular components of the laser field, ω_{las} – the frequency of the laser light, $\vec{k}$ – the wave vector.

The relaxation of the atomic system is described phenomenologically by the sum of two terms and in the general case includes radiation and collisions processes. The first term describes the decay constants $\Gamma_\rho(\kappa)$ $(\rho = f, \varphi, \xi)$ for the k-th tensor component of the upper (f) and lower (φ) levels and the decay of the optical coherence (ξ). The decay of the lower level $\Gamma_\varphi(0)$ includes the time-of-flight. The second term $(\dot{\hat{\rho}})_{\text{tr}}$ describes the excitation transfer by spontaneous emission $\Gamma_{f\varphi}(\kappa)$ from the upper level to the lower one and includes the transfer of Zeeman coherence.

The relaxation constant $\Gamma_{F_f F_\varphi}(k)$ describes the "losses" in the channel $F_f \rightarrow F_\varphi$. According to Ducloy [14] and taking into account Dyakonov's normaliza-

tion of the irreducible tensor operators [15]

$$\Gamma_{_{F_f F_\varphi}}(k) = (-1)^{F_f+F_\varphi+k+1}\Big[\gamma_f(0)(2F_f+1)(2F_\varphi+1)(2J_f+1)\Big] \times \left\{ \begin{array}{ccc} F_f & F_\varphi & 1 \\ J_\varphi & J_f & I \end{array} \right\}^2 \sqrt{(2F_f+1)(2F_\varphi+1)} \left\{ \begin{array}{ccc} F_f & F_f & k \\ F_\varphi & F_\varphi & 1 \end{array} \right\}, \quad (3)$$

where $\gamma_f(0)$ is the full probability for upper level F_f decay to all lower ones. If the branching ratio $\Gamma_{_{F_f F_\varphi}}(0)/\gamma_f(0)$ is close to 1 the atomic system is closed. In the particular case of ^{87}Rb, D_1 line transition $F_f = 1 \rightarrow F_\varphi = 2$, the ratio $\Gamma_{_{F_f F_\varphi}}(0)/\gamma_f(0) = 5/6$.

For the matrix element of the dipole transitions between hf states in ITO representation one can write [2]

$$d_{_{F_f F_\varphi}} = \|d_{f\varphi}\|(-1)^{2F_\varphi+J_f+I+1}\left[(2F_f+1)(2F_\varphi+1)\right]^{1/2} \times \left\{ \begin{array}{ccc} I & J_f & F_f \\ 1 & F_\varphi & J_\varphi \end{array} \right\} (-1)^{F_\varphi+m} \left\{ \begin{array}{ccc} F_\varphi & 1 & F_f \\ -m & Q & \mu \end{array} \right\} e_Q\,. \quad (4)$$

The initial conditions are defined by the operator $\hat{N} = N_s(2F_s+1)W(v)$, which describes the population of the levels coupled by the laser light. It is supposed that the atomic ensemble is in equilibrium and the velocity distribution of the atoms is described by the Maxwell function $W(v)$.

$$W(v) = \left(u\sqrt{\pi}\right)^{-1} e^{(-v^2/u^2)}\,. \quad (5)$$

The operator $\hat{N}$ gives the normalization of the density matrix.

Taking into account the stated above, we can write down the system of equations for the tensor components $\rho_q^k(\rho = f, \varphi, \xi)$ describing a ground state (φ) and an exited state (f), and the optical coherence (ξ) for arbitrary angular momenta is derived (see details for instance in [16]).

Interaction with arbitrary oriented E and B fields was written down in details aiming to simplify modelling of the influences of the stray magnetic fields and different geometries and parameters of the experiment

3 Numerical Modelling

In most theoretical works the calculations are performed in adiabatic approximation or broad line approximation (BLA) [8,17]. The analysis of K. Blushs and M. Auzinsh [17] shows that the solutions of the stationary Bloch equations describe very well coherent resonances in a strong laser field and continuous excitation without the need of additional equation limitations. This requirement means that

the processes of laser excitation and interaction with a magnetic field are slower than all relaxation rates in the system. The optical coherences oscillate with the frequency of the laser field, and after substituting

$$\xi_q^\kappa(t) = \tilde{\xi}_q^\kappa \exp\{i(\omega_{\text{las}} t - kz)\}; \qquad f_q^\kappa = \tilde{f}_q^\kappa, \qquad \varphi_q^\kappa = \tilde{\varphi}_q^\kappa, \qquad (6)$$

we obtain a system of algebraic equations for the new components. To calculate the coefficients in the equations we need the mean quantum numbers of the resonance transition, the geometry of excitation and the directions of the stray and scanned magnetic fields.

The quantization axis in all our calculations was chosen parallel to the electric vector $\vec{E}(\equiv E_z \equiv E\,\vec{e}_0)$ of the laser field. The scanned magnetic field $B_{\text{scan}}(\equiv B_x)$ is perpendicular to this axis. The influence of the laboratory magnetic field is taken into account including two magnetic components B_z and B_y.

The quantities characterizing the atomic system and the excitation laser field – relaxation constants $\Gamma_\rho(\kappa)$ $(\rho = f, \varphi, \xi)$, Rabi frequency $(\Omega_R = dE/h)$, detuning of the laser frequency from the resonance transition frequency $\Delta\omega = \omega_{f\varphi} - \omega_{\text{las}}$ and the initial level populations (N_f, N_φ) are parameters in the equations and can be varied corresponding to the experimental conditions. The stray magnetic field is introduced as a parameter too.

The number n of the equations depends on the chosen transition and is determined as $n = 4[F_f + F_\varphi + 1]^2$. The simplest case of CPT transition $F_f = 0 \rightarrow F_\varphi = 1$, $(n = 16)$ was used as a test for the method chosen for algebralization of the system of equations. Such system of equations can be solved with the full set of parameters if the atom velocity distribution is not

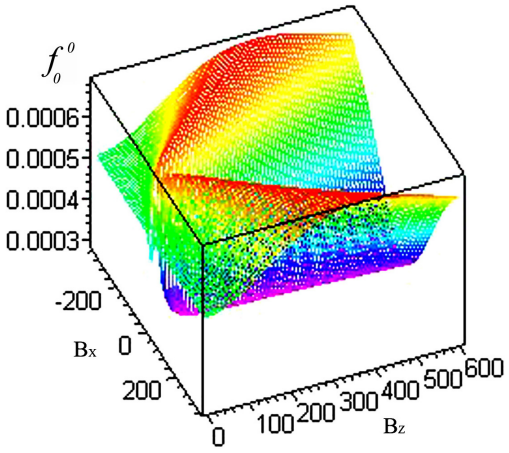

Figure 1. Upper level population f_0^0 dependence on the scanned (B_x) and stray (B_z) magnetic fields for $F_f = 0 \rightarrow F_\varphi = 1$ transition.

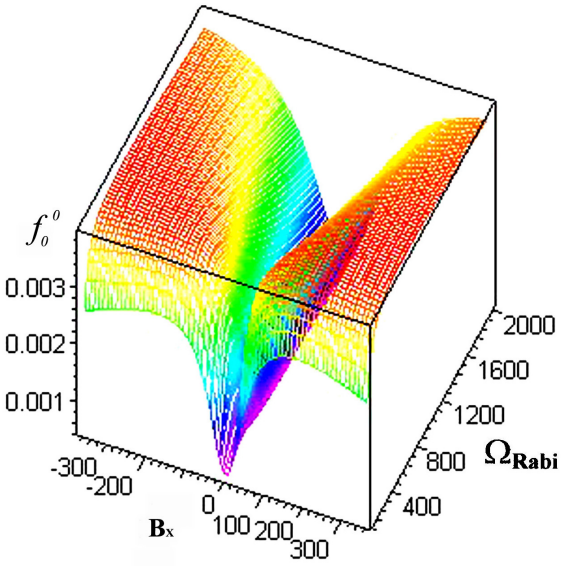

Figure 2. CPT resonance narrowing in dependence on the Rabi frequency in the presence of a stray magnetic field $B_z = 0.2\Gamma_f(0)$ for $F_f = 0 \rightarrow F_\varphi = 1$ transition.

taken into account. The obtained multi-parametric solutions for each of the 16 tensor components can be analyzed by varying any of the parameters. In Figure 1 a 3D example is shown of the upper level population dependence f_0^0 on the scanned B_x and stray B_z magnetic fields. The magnetic fields are presented in $10^{-3}\Gamma_f(0)$ units, the Rabi parameter is $0.2\Gamma_f(0)$ and the frequency detuning – $4\Gamma_f(0)$. From the figure it is seen that the stray magnetic field, directed along the electrical vector E, strongly broadens the resonance at a strong magnetic field, but at weak field it nonlinearly increases in amplitude. When the Rabi frequency is a variable parameter, at fixed stray magnetic field of $0.2\Gamma_f(0)$ and zero detuning from the resonance frequency, narrowing of the CPT resonance and following saturation of its amplitude is obtained.

In a real experiment on the resonance Rb and Cs transitions the number of equations increases significantly and it becomes difficult to find multi-parametrical solutions. For better description of the real experimental conditions, the program is additionally modified to take into account the Maxwell velocity distribution of the atoms in the cell, and the Gaussian (or other) intensity distribution of the irradiating beam.

The corresponding algebraic system of equations was calculated for a given transition and geometry. The numerical experiments were performed for the $F_f = 1 \rightarrow F_\varphi = 2$ transition of Rb varying the corresponding parameters. The solutions for all 64 tensor components allow visualizing the connections between them and the dynamics of the influence of the varied parameters.

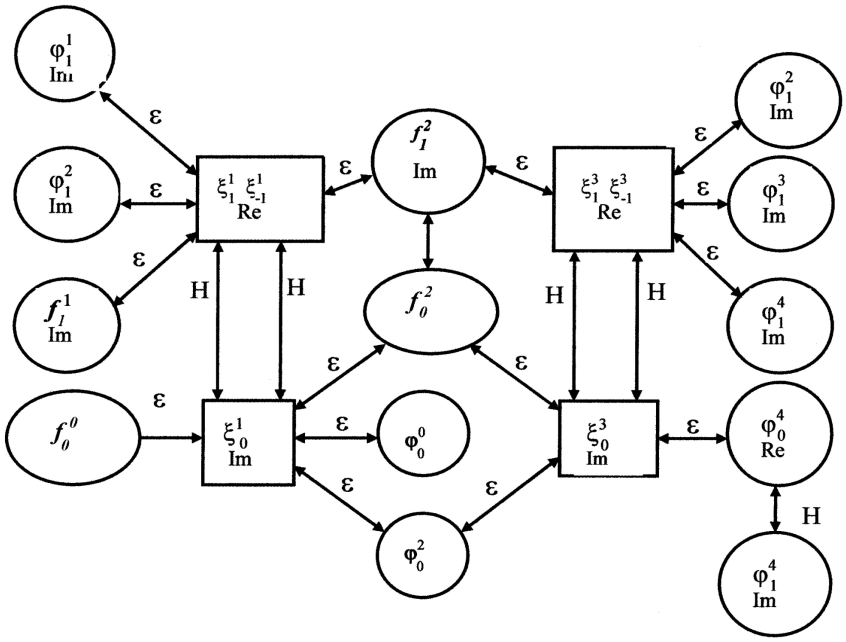

Figure 3. Partial scheme of the mutual conversion of the tensor components representing the population and longitudinal alignment. ε and H denotes the interaction with the laser and magnetic field respectively.

The partial scheme of connections for upper level population and alignment f_0^0, f_q^2, $(q = 0, \pm 2)$ due to the interaction with the laser and magnetic fields are shown in Figures 3 and 4. In accordance with the choice of quantalization axes the laser field connects the tensor components with equal q indexes ($\varphi_{-q}^k = (-1)^q(\varphi_q^k)^*$). The coherence in the system with such geometry is created by the scanned magnetic field which connects the tensor components with different q ($\Delta q = \pm 1$). The sequence of the connections shows the possible channels for conversion of the non-observable tensor components having rank $k > 2$ (octopole and hexadecapole moments) into observable in the fluorescence ones.

Comparing the two systems, it is seen that they are partially overlapped and complement each other. Of importance is that the optical components with rank higher than 2, and through them the hexadecapole moments φ_q^4, convert into the transverse alignment Re f_2^2. Hence, narrower resonance structures should be observed

The non-Doppler solutions obtained through variation of the parameters allow practically immediately to estimate the influence of each given parameter on the observable tensor components. Using the obtained results one can plan numerical calculations, which model the real experiment (taking into account the

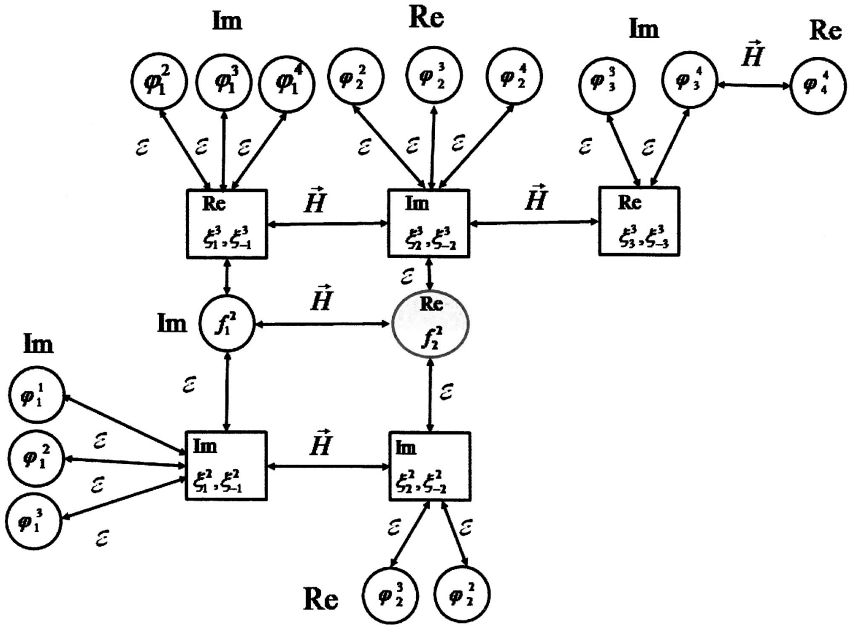

Figure 4. Partial scheme of the mutual conversion of the tensor components into transversal alignment, where ε and H denotes the interaction with the laser and magnetic field respectively.

atomic velocity distribution, the parameters of the atomic system and the geometry of the real experiment)

The presented Matlab based program allows resonance visualization in the region close to the zero magnetic field ($\pm$ several mG). It consists of separate blocks for virtual experiment modelling – 4 in our case.

Block integration in one computation process is realized by a script file. It contains the initial parameter values for the considered transition: value of the stray magnetic field, range of the scanned magnetic field, parameters of the laser field and its frequency detuning from the resonance frequency; Doppler width, the maximal and minimal value of the scanning step. To speed up the computing, the scanning step is set variable – from the minimum value near the resonance to a maximum value for the Doppler curve wings. These sets are accepted by default at the first step of calculation.

After that a user menu is introduced. It shows the initially established parameters of the virtual experiment and allows changing the parameter values and correcting the errors. Sparse-matrix for all equations for the relaxation parameters is composed.

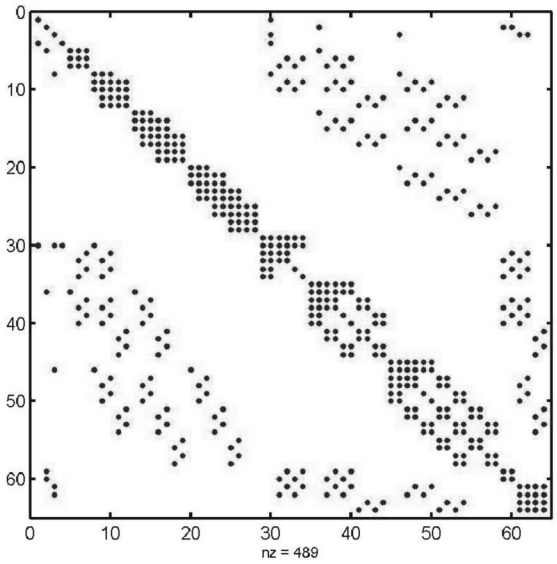

Figure 5. Non-zero matrix elements for the $F_\varphi = 2 \rightarrow F_f = 1$ transition.

The third block creates the basic matrix, consisting of sub-matrices. Each sub-matrix depends on one given parameter – Ω_{Rabi}, B_y, B_z, $(\omega_{\text{las}} - \omega_{f\varphi})$, B_{scan} (in units $\gamma_f(0)$). The basic matrix can be visualized and it is possible to check its proper writing. The basic matrix written for $F_\varphi = 2 \rightarrow F_f = 1$ transition is shown in Figure 5.

Computation for each given parameter is performed following the same algorithm.

The solution for a given variable (ρ_q^k) is taken after summarizing the partial solutions for the sub-ensemble of atoms with velocities in a given interval. The integration region is chosen to be $> 40\Gamma_f(0)$, and the integration step is varied. The obtained solutions for a given Rabi frequency are also averaged over the intensity distribution of the beam.

4 Examples of Numerical Simulation and Comparison with Experiments

In a typical CPT experiment in Hanle configuration the dependence of the fluorescence or absorption on a scanned magnetic field is detected. In a dipole approximation the fluorescence and absorption are defined only by the tensor components ρ_q^k with rank $k \leqslant 2$. The unpolarized fluorescence intensity, which

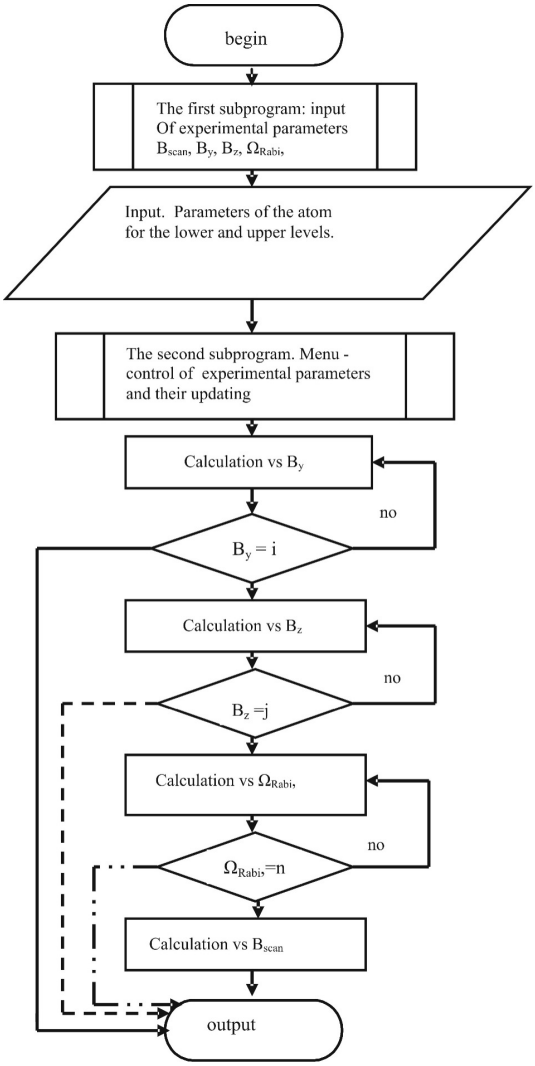

Figure 6. Calculation algorithm schematic diagram.

is usually registered in a standard experiment, can be written as

$$I_{f\varphi}(\text{unpol}) = C_0 \left[\frac{f_0^0}{\sqrt{2F_f+1}} + (-1)^{F_f+F_\varphi+1}\sqrt{30} \begin{Bmatrix} 1 & 1 & 2 \\ F_f & F_f & F_\varphi \end{Bmatrix} f_0^2 \right]. \quad (7)$$

Only the two tensor components f_0^0 and f_0^2 describe the observed signal in an unpolarized fluorescence and the main part of the intensity is determined by the population (f_0^0).

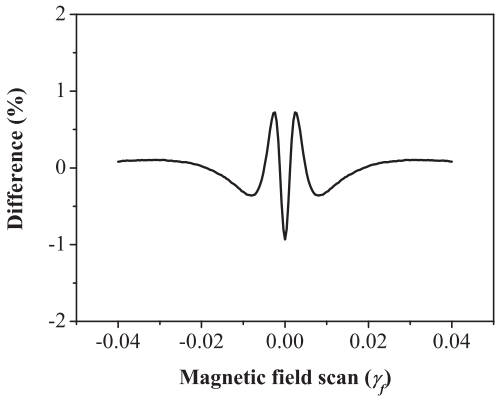

Figure 7. Difference between the calculated resonance line shape and its Lorentzian profile fit at $\Omega_R = 1$ MHz ($\sim 0.2\gamma_f$).

Using the approach described above the influence of the high rank polarization moments on the CPT resonance shape was modelled and checked experimentally.

If only the Maxwell velocity distribution of the atoms is taken into account, the theoretical resonance of the shape remains quasi Lorentzian. In the case of power densities corresponding to Rabi frequencies of the order of 1 MHz ($\sim 0.2\gamma_f$), the calculated CPT resonance the shape could not be visually distinguished from a Lorentzian, but in the difference between the calculated profile and its Lorentzian fit there was a specific structure at the center [6,18]. (Figure 7). This difference corresponds to multiphoton resonances. Although the

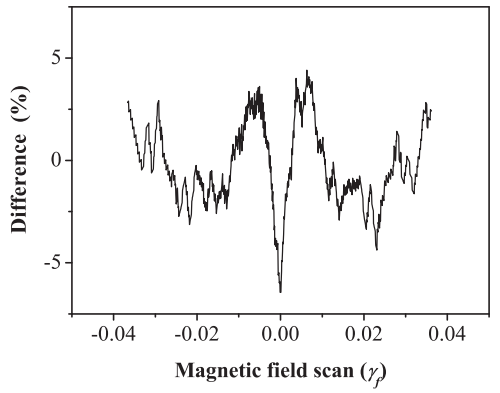

Figure 8. Line shape difference between the experimental resonance and its Lorentzian fit at $\Omega_R = 1$ MHz.

moment of rank $k > 2$ do not influence directly the spontaneous emission, they convert into components of the upper level of rank 2 f_q^2 and in this way influence the spontaneous emission (see Figures 3,4).

Measurements of the CPT resonance lineshapes were performed to check the lineshapes obtained theoretically. At a power density of 1.7 mW/cm^2 (for a laser linewidth 50 MHz, corresponding to reduced Rabi frequency $\Omega_R = 1$ MHz), the measured CPT resonance lineshape was close to Lorentzian. The difference between the experimental profile and its Lorentzian fit is presented in Figure 8 [18].

The shape and amplitude of this structure are similar to the one reported in [7] and to the theoretical ones (Figure 7). The difference around zero magnetic field is a result of the influence of the HRPM, which is included in our model [18] and is not included in the other one [7].

Another way to observe the contribution of the converted HRPM components to the CPT resonance is to use the classical for Hanle effect scheme, registering differential signal of 2 orthogonal polarizations of the spontaneous emission. In this case, the signal is determined by the transverse component of the alignment $f_{\pm 2}^2$, which includes the converted high-rank polarization moments (see Figures 3, 4). As this signal excludes the contribution of the population, its amplitude has to be about an order of magnitude smaller, and about two times narrower. This narrow part originates from the hexadecapole moments (φ_q^4).

Figure 9 shows an example of experimentally obtained CPT-resonances for two orthogonal polarizations (PhD1, PhD2) together with the differential signal (PhD1-PhD2) and magnetic field scan [19]]. The differential signal is signifi-

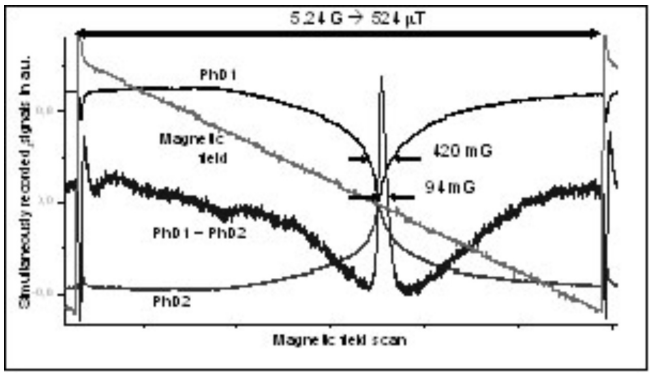

Figure 9. Simultaneously recorded dependence of the orthogonally polarized spontaneous intensity I_x and I_y on the magnetic field (photo-detectors PhD1 and PhD2 respectively) and their difference (PhD1 – PhD2). The magnetic field sweep of 5.24 G symmetrically around zero value.

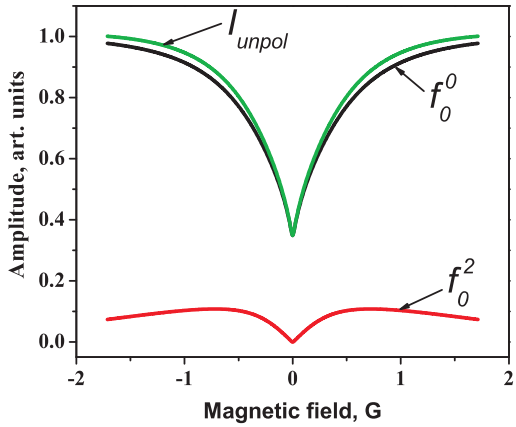

Figure 10. Influence of the longitudinal alignment on the CPT resonance lineshape.

cantly narrower than the signals from the direct registration of the fluorescence. The shape of the differential signal corresponds to the theoretically calculated one. The qualitative agreement between the shapes of the calculated and experimentally obtained resonance confirms the correctness of the selected approach. The resonance narrowing obtained with this simple method can be used to improve the sensitivity of magnetic field measurements

The program described above was applied to estimate also the influence of the longitudinal alignment on the shape of the resonance. The influence of the Gaussian distribution of the laser beam intensity, discussed in many papers [6-8,20] was examined too. As can be seen from (Figure 10) f_0^2 slightly changes the

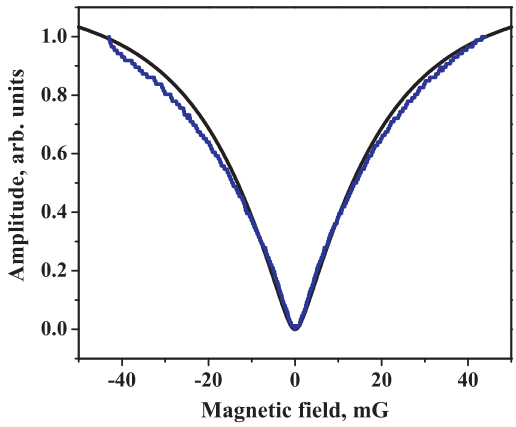

Figure 11. CPT resonance lineshapes: theoretical (black) and experimental (blue) ones.

curve wings and does not actually change the resonance width.

The theoretical curve, obtained after numerical calculations taking into account the Maxwell velocity distribution and the Gaussian distribution of the laser beam and experimental one, obtained at power density 1200 W/m^2 ($\Omega_R = 25$ MHz), are compared in Figure 11. The typically triangle line shape is in accordance with the experiment (see for example also signals PhD1, 2 in Figure 9)

5 Conclusion

A model for numerical calculations of the CPT-Hanle configuration resonances, which uses the ITO formalism and takes into account the influence of the velocity distribution of the atoms, the Gaussian distribution of laser beam intensity and the HRPM is developed. The Matlab based programs allow performing simulations of the experiments by varying different parameters. The mutual conversion of the HRPM into observable quadrupol moments is visualized. The comparison of the obtained theoretical line shape of the resonances with experiments shows good agreement

Acknowledgement

The authors are pleased to acknowledge the financial support of the NFSR Grant DO–02–108.

References

[1] J. Dupon-Roc, S. Haroche, C. Cohen-Tannoudji (1969) *Phys. Lett.* **28A** 638.

[2] E.B. Alexandrov, M.P. Chaika, G.I. Hvostenko (1991) "Interference of atomic states", Springer-Verlag.

[3] G. Alzetta, A. Gozzini, L. Moi, G. Orriols (1976) *Nuovo Cimento* **B36** 5-20.

[4] H.Y. Ling, Y.-Q. Li, M. Xiao (1996) *Phys. Rev. A* **53** 1014-1026.

[5] C. Andreeva, S. Cartaleva, Y. Dancheva V. Biancalana, A. Burchianti, C. Marinelli, E. Mariotti, L. Moi, K. Nasyrov (2002) *Phys. Rev. A* **66** 012502.

[6] E. Pfleghaar, J. Wurster, S.I. Kanorsky, A. Weis (1993) *Opt. Commun.* **99** 3003.

[7] A.V. Taichenachev, A.M. Tumaikin, V.I. Yudin (2004) *Phys. Rev. A* **69** 024501.

[8] B. Decomps, M. Dumont, M. Ducloy (1976) In: "Laser Spectroscopy of Atoms and Molecules" (Topics in Applied Physics Vol. 2 – Springer Verlag) 283-347; DOI: 10.1007/3-540-07324-8_11

[9] V.V. Yashchuk, D. Budker, W. Gawlik, D.F. Kimball, Y.P. Malakyan, S.M. Rochester (2003) *Phys. Rev. Lett.* **90** 253001.

[10] A.M. Okunevich (2001) *Optics and Spectroscopy* **91** 177183. Translated from *Optika i Spektroskopiya* **91** (2001) 193200.

[11] L. Petrov, D. Slavov, V. Arsov, V. Domelunksen, V. Polischuk, G. Todorov (2007) *Proc. SPIE* **6604** 66040H.

[12] M. Auzinsh, R. Ferber, F. Gahbauer, A. Jarmola, L. Kalvans (2009) *Phys. Rev. A* **79** 053404.

[13] K.A. Nasirov (2010) *Avtometry* **46** 54-63 (in Russian).

[14] M. Ducloy, M. Dumont (1970) *J. de Physique* **31** 419-427.

[15] M.I. D'yakonov, V.I. Perel (1966) *Optics and Spectroscopy* **20** 101.

[16] A. Huss, R. Lammegger, L. Windholz, E. Alipieva, S. Gateva, L. Petrov, E. Taskova, G. Todorov (2006) *JOSA B* **23**(9) 1729-36.

[17] K. Blushs, M. Auzinsh (2004) *Phys. Rev. A* **69** 063806.

[18] S. Gateva, L. Petrov, E. Alipieva, G. Todorov, V. Domelunksen, V. Polischuk (2007) *Phys. Rev. A* **76** 025401.

[19] D. Slavov, L. Petrov, M. Balabas, V. Domelunksen, V. Polischuk, G. Todorov (2009) *Compt. Rendus de l'Acad. Bulg. des Sci.* **62** 1067-73.

[20] F. Levi, A. Godone, J. Vanier, S. Micalizio, G. Modugno (2000) *Eur. Phys. J.* **D12** 53-59.